Broadband femtosecond lasers enable efficient two-photon excitation of the ultranarrow linewidth singlet 1*s*2*s* state in helium

Shashank Kumar [1,*] Justin D. Piel [1] Chris H. Greene [1,2] and Niranjan Shivaram [1,2,†]
[1]*Department of Physics and Astronomy, Purdue University, West Lafayette, Indiana 47907, USA*
[2]*Purdue Quantum Science and Engineering Institute, Purdue University, West Lafayette, Indiana 47907, USA*

(Received 18 September 2025; accepted 10 December 2025; published 8 January 2026)

We propose a broadband, femtosecond two-photon excitation scheme for efficient population transfer to the ultranarrow linewidth $1s2s\ ^1S_0$ metastable state in helium. Using 120 nm vacuum ultraviolet femtosecond laser pulses, we theoretically demonstrate that a direct two-photon excitation process can achieve a population transfer efficiency of 25%–30%, even when photoionization losses are included. The use of broadband pulses enables multiple excitation pathways to populate the excited state, in addition to compensating for significant ac Stark shifts occurring within the pulse duration. Furthermore, we introduce a two-color two-photon extreme-ultraviolet-near-infrared (XUV-IR) excitation scheme that will further reduce ionization losses and can achieve significantly higher transfer efficiencies of ∼70%. These results demonstrate that high excitation probability of ultranarrow linewidth (∼50 Hz) excited states can be achieved using experimentally accessible femtosecond laser sources with bandwidth in the terahertz range.

DOI: 10.1103/nfbf-h6hc

I. INTRODUCTION

Narrow linewidth atomic states play a central role in quantum technologies, precision metrology, and advanced spectroscopy. Their long lifetimes allow coherent population control, a prerequisite for realizing long-lived qubits [1–6] and high-precision atomic and nuclear clocks [7–11]. Among the most prominent examples are the metastable $2s\ ^2S_{1/2}$ state of atomic hydrogen (and hydrogenlike systems) and the $1s2s\ ^1S_0$ state of atomic helium, both of which exhibit lifetimes on the order of milliseconds [12–16]. The longest-lived neutral atomic state is the first triplet excited state of helium, $1s2s\ ^3S_1$, which has a lifetime of ∼7800 s [17]. Owing to their ultranarrow linewidths, these states allow for extremely accurate determinations of transition frequencies. In particular, the 1*s*–2*s* transition in atomic hydrogen [18–20] and antihydrogen [21] has been measured with exceptional precision. These long-lived states primarily decay via two-photon emission [13,22–25]. A recent study suggests that the emitted photons could serve as a source of attosecond entangled biphotons [26].

However, laser-assisted population transfer to a narrow linewidth atomic state has long posed an experimental challenge. Narrow bandwidth π pulses are typically used to coherently populate these metastable states [21,27], and similar approaches have been employed to excite atoms into Rydberg states [28,29]. In practice, however, dynamic Stark shifts of the atomic levels and laser instabilities often limit the transfer efficiency. The requirement of narrow spectral bandwidths makes efficient transfer with a single pulse impractical, motivating the development of multipulse techniques. One widely established method is stimulated Raman adiabatic passage (STIRAP), which employs a delayed pulse sequence to adiabatically transfer the population from the initial to the final state while avoiding population of the intermediate state [30–32]. Another, theoretically proposed approach, is the Stark-chirped rapid adiabatic passage (SCRAP), in which a multiphoton excitation pulse is combined with a delayed nonresonant pulse that induces a Stark shift to facilitate adiabatic transfer [33–35]. Moreover, in many atomic and molecular systems, the ground-to-first-excited-state energy gap lies in the vacuum-ultraviolet (VUV) or extreme-ultraviolet (XUV) regime, where generating nanosecond pulses with sufficient power remains experimentally challenging, making efficient creation of excited states difficult in this regime.

In recent years, great advances have been made in generating VUV femtosecond pulses using techniques such as high-harmonic generation [36,37], wave mixing processes [38,39], white-light supercontinuum formation [40,41], and frequency-tunable resonant dispersive wave (RDW) emission [42–48]. With broadband VUV pulses now readily available, two-photon excitation in large energy-gap systems, such as helium, has become experimentally feasible. However, the high peak intensities of femtosecond lasers (on the order of $\mathrm{TW/cm^2}$) inevitably drive strong multiphoton ionization, which severely limits population transfer efficiency. This presents a major hurdle for applications where high excitation probabilities of narrow excited states are required [26].

*Contact author: kumar414@purdue.edu
†Contact author: niranjan@purdue.edu

Published by the American Physical Society under the terms of the Creative Commons Attribution 4.0 International license. Further distribution of this work must maintain attribution to the author(s) and the published article's title, journal citation, and DOI.

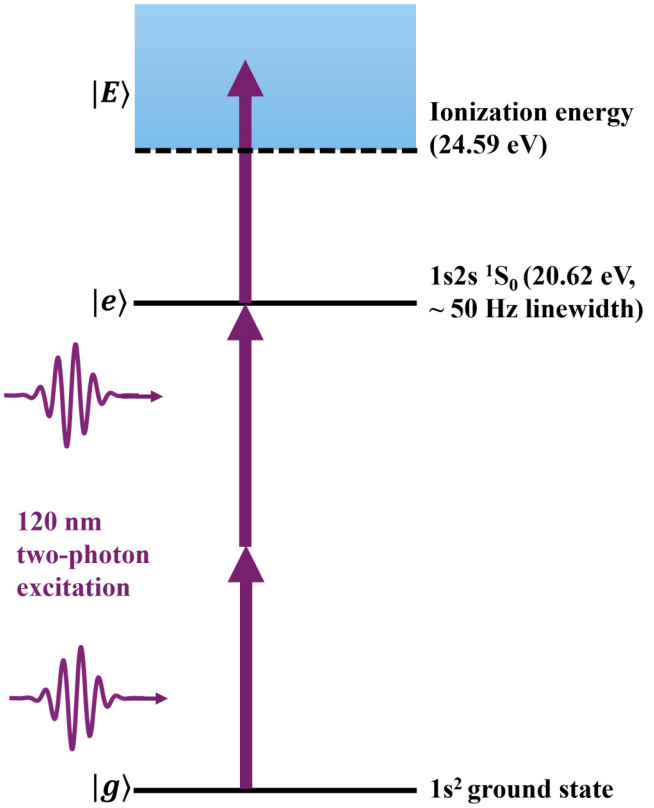


FIG. 1. A two-photon excitation scheme with femtosecond 120 nm pulses, including photoionization of the $1s2s\ ^1S_0$ state of the helium atom.

In the present work, we investigate two-photon excitation in the helium atom using broadband femtosecond laser pulses, showing that such pulses can achieve high population transfer to the $1s2s\ ^1S_0$ state with ultranarrow linewidth (∼50 Hz), despite the large bandwidth (∼1 THz) and typically high multiphoton ionization rates of femtosecond pulses. In Sec. II, we derive an effective two-level Hamiltonian that depends on the dynamic Stark shifts, the two-photon Rabi frequency, and the ionization rate. Section III presents numerical solutions of this model for varying femtosecond pulse parameters (intensity and spectral bandwidth), from which we identify experimentally accessible regimes that maximize population transfer. In Sec. IV, we introduce a two-color, extreme-ultraviolet and near-infrared (XUV—IR) two-photon excitation scheme, which results in high excitation probabilities of ∼70%. Finally, we conclude this article in Sec. V.

II. THEORY OF TWO-PHOTON EXCITATION

In this section, we present the theoretical framework for two-photon excitation of a helium atom by a broadband pulse. The system consists of the ground state $1s^2$ and the first excited state $1s2s\ ^1S_0$ of the helium atom, separated by 20.62 eV. Because both states have the same parity ($l = 0$), a single-photon dipole transition is forbidden, and excitation requires the absorption of two photons (see Fig. 1). Since our primary focus is on the final population of the $1s2s$ state, the framework also incorporates photoionization pathways that compete with the two-photon excitation process. The total Hamiltonian is written as $H = H_0 + V(t)$, where H_0 is the field-free atomic Hamiltonian. Its eigenenergies and eigenfunctions are obtained using finite-volume variational R-matrix methods [49], which are well established to accurately describe helium excitation and ionization continua. The laser-atom interaction is treated within the dipole approximation, $V(t) = -\boldsymbol{\mu} \cdot \boldsymbol{E}_P(t)$, where $\boldsymbol{\mu}$ is the dipole operator and $\boldsymbol{E}_P(t)$ is the pump electric field. For a femtosecond laser pulse, the field takes the form

$$\boldsymbol{E}_P(t) = \boldsymbol{\varepsilon}_P(t)\cos(\omega_P t), \tag{1}$$

with $\boldsymbol{\varepsilon}_P(t)$ denoting the Gaussian envelope and ω_P the central angular frequency. The temporal phase is assumed to be zero. In Fig. 1, we consider a pulse with central wavelength 120.27 nm, corresponding to $\hbar\omega_P = 10.31$ eV, such that two-photon absorption matches the $1s^2 \rightarrow 1s2s$ excitation. Later, we will also analyze a two-color excitation scheme, where the two absorbed photons have different frequencies. Unless stated otherwise, the following Gaussian intensity profile is used throughout this article:

$$I(t) = I_0 \exp\left(-4\ln 2\frac{t^2}{\tau^2}\right), \tag{2}$$

where τ is the full width at half maximum (FWHM) and I_0 is the peak intensity of the excitation pulse. The envelope function of the electric field can be determined by using the relation $I = \frac{1}{2}\epsilon_0 c\varepsilon_P^2$.

The total time-dependent wave function for such a system can be written as

$$|\psi\rangle = c_g e^{-i\omega_g t}|g\rangle + c_e e^{-i\omega_e t}|e\rangle + \sum_m c_m e^{-i\omega_m t}|m\rangle + \int dE\ c_E(t)e^{-i\omega_E t}|E\rangle. \tag{3}$$

Here, $|g\rangle$ denotes the ground state, $|e\rangle$ the excited state $1s2s\ ^1S_0$, and $|E\rangle$ the continuum states. $|m\rangle$ represents intermediate p states that mediate the two-photon excitation, but are omitted for the sake of clarity in Fig. 1. Substituting Eq. (3) into the time-dependent Schrödinger equation yields the coupled rate equations for the complex amplitudes $c_i(t)$.

$$i\hbar\dot{c}_g(t) = \sum_m c_m(t)e^{-i\omega_{mg}t}V_{gm}(t), \tag{4a}$$

$$i\hbar\dot{c}_e(t) = \sum_m c_m(t)e^{-i\omega_{me}t}V_{em}(t) + \int dE\, c_E(t)e^{-i\omega_{eE}t}V_{eE}(t), \tag{4b}$$

$$i\hbar\dot{c}_m(t) = \sum_{j=g,e} c_j(t)e^{i\omega_{mj}t}V_{mj}(t), \tag{4c}$$

$$i\hbar\dot{c}_E(t) = c_e(t)e^{i\omega_{Ee}t}V_{Ee}(t), \tag{4d}$$

where $V_{ij}(t) = -\langle i|\boldsymbol{\mu}\cdot\boldsymbol{E}_P(t)|j\rangle$ is the dipole interaction matrix element and $\omega_{ij} = \omega_i - \omega_j$. Since the transition to intermediate states $|m\rangle$ is off resonant, the highly oscillating time-dependent amplitudes can be evaluated using adiabatic elimination [50]. Equation (4c) can then be integrated to

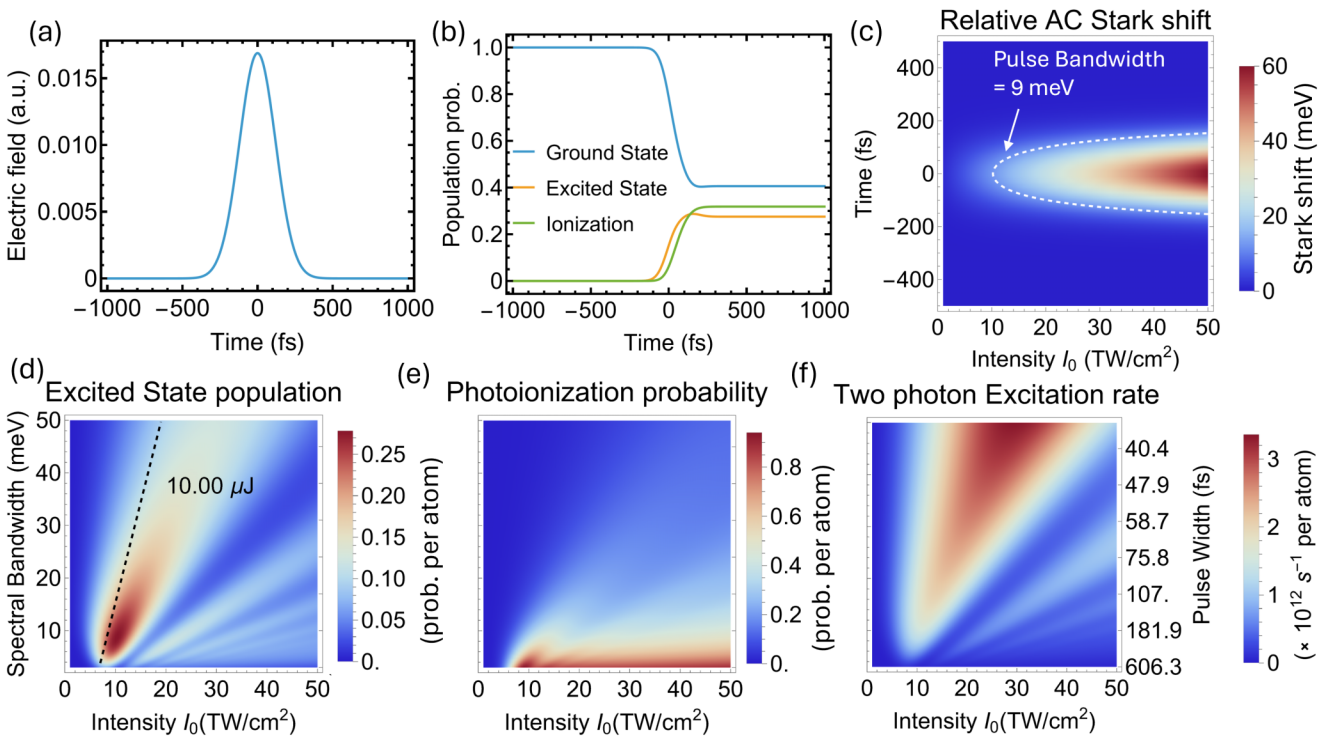


FIG. 2. (a) The electric field profile of the pump (excitation) laser. (b) The time evolution of the ground-state (blue curve) and the excited-state (orange curve) population in the presence of the pump laser electric field. The ionization probability is also shown as a green curve. (c) The relative ac Stark shift, i.e., difference between the time-dependent Stark shift of the ground and the $1s2s\ ^1S_0$ excited state, is shown as a function of pulse intensity with the pulse bandwidth fixed to 9 meV. The white dashed line represents a 9 meV contour where the relative ac Stark shift matches the pulse bandwidth. (d) The excited-state population $P_e(t = 1000\ \text{fs})$ is shown in the parameter space of intensity and pulse spectral bandwidth (full width at half maximum). The dashed line is for constant pulse energy = 10 μJ. (e) The fraction of He atoms that are photoionized is $1 - |c_g|^2 - |c_e|^2$. (f) The two-photon excitation rate. The Fourier-transform limited pulse width of the pump laser is labeled on the right side of the y axis. The detuning in all the plots is $\Delta = 2\omega_P - \omega_{eg} = 14.3$ meV.

obtain

$$c_m(t) \approx \sum_{j=g,e} \frac{c_j \mu^P_{mj}}{2\hbar}\left[\frac{\varepsilon_P e^{-i(\omega_P-\omega_{mj})t}}{\omega_{mj}-\omega_P} + \frac{\varepsilon^*_P e^{i(\omega_P+\omega_{mj})t}}{\omega_{mj}+\omega_P}\right], \quad (5)$$

where $\mu^P_{mj} = \langle m|\boldsymbol{\mu}\cdot\hat{e}_P|j\rangle$ is the dipole matrix element projected along the polarization direction of the pump pulse. Similarly, Eq. (4d) governs the time evolution of the continuum amplitudes;

$$c_E(t) = \frac{-1}{2i\hbar}\int_{-\infty}^{t} dt' c_e(t')\mu^P_{Ee}[\varepsilon_P e^{-i(\omega_P-\omega_{Ee})t} + \varepsilon^*_P e^{i(\omega_P+\omega_{Ee})t'}]. \quad (6)$$

Now, substituting these amplitudes into Eqs. (4a) and (4b), we obtain the coupled differential equations for the amplitudes $c_g(t)$ and $c_e(t)$. Within the rotating-wave approximation (RWA) and the two-photon RWA, where rapidly oscillating terms beyond the two-photon detuning $\Delta = 2\omega - \omega_{eg}$ are neglected, this simplifies to

$$i\begin{pmatrix}\dot{c}_g\\ \dot{c}_e\end{pmatrix} = \begin{pmatrix} S_g(t) & \frac{\Omega^{P*}_{ge}}{2}e^{i\Delta t}\\ \frac{\Omega^P_{ge}}{2}e^{-i\Delta t} & S_e(t) + \frac{\delta E_e}{\hbar} - \frac{i}{2}\Gamma^P_e\end{pmatrix}\begin{pmatrix}c_g\\ c_e\end{pmatrix}. \quad (7)$$

Here, $\hbar S_{g/e}$ is the dynamical Stark shift of the ground/excited state and is given by

$$S_j(t) = -\sum_m \frac{|\mu^P_{mj}|^2}{2\hbar^2}|\varepsilon_P|^2\frac{\omega_{mj}}{\omega^2_{mj}-\omega^2_P}. \quad (8)$$

The effective two-photon Rabi frequency coupling the ground state and the excited state can be expressed as

$$\Omega^P_{ge} = -\sum_m \frac{\mu^P_{em}\mu^P_{mg}}{2\hbar^2}\frac{\varepsilon^2_P(t)}{\omega_{mg}-\omega_P}. \quad (9)$$

The term δE_e represents the dynamical energy shift of the $1s2s$ state arising from its coupling to the continuum, while Γ^P_e denotes the photoionization rate of the excited state $1s2s$ [51,52]:

$$\delta E_e = -\mathcal{P}\int dE \frac{1}{4\hbar}\frac{|\mu^P_{eE}|^2|\varepsilon_P|^2}{\omega_E-\omega_P-\omega_e}, \quad (10)$$

$$\Gamma^P_e(t) = \frac{\pi}{2\hbar}|\varepsilon_P|^2|\langle e|\mu\cdot\hat{e}_P|E = \hbar\omega_P + \hbar\omega_e\rangle|^2, \quad (11)$$

where $\mathcal{P}$ indicates the principal value.

III. TIME EVOLUTION OF POPULATION

After applying adiabatic elimination, Eq. (7) is solved numerically using the explicit Runge-Kutta method. Figure 2(a)

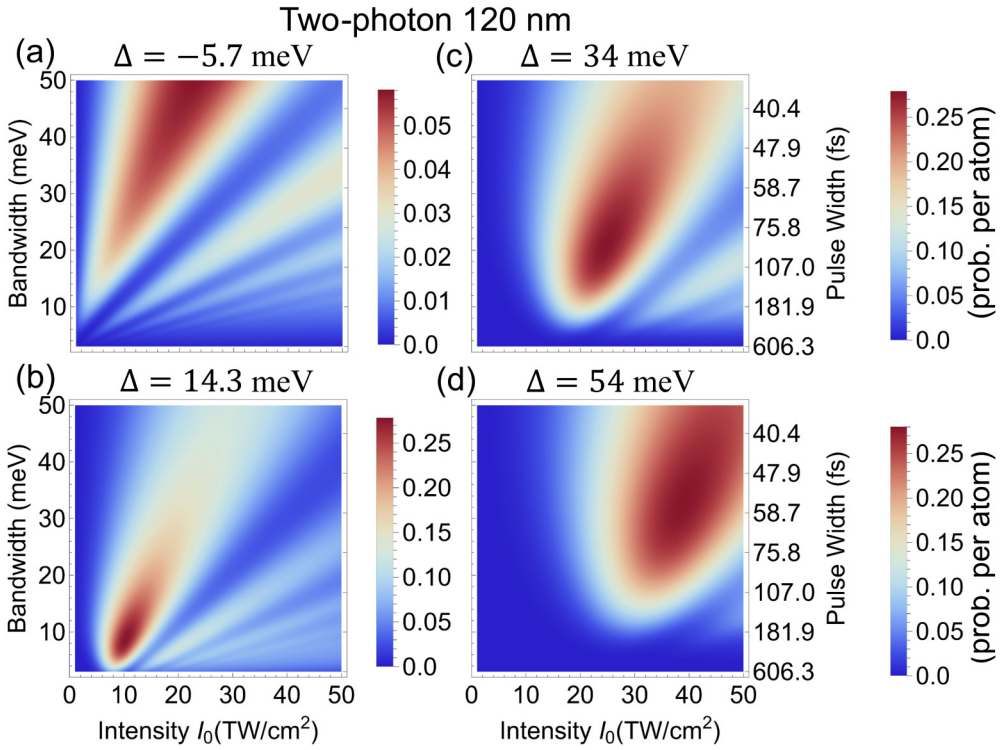


FIG. 3. The excitation probability as a function of pump intensity and pulse width for various two-photon detuning $\Delta = 2\omega_P - \omega_{eg}$: (a) $\Delta = -5.7$ meV, (b) $\Delta = 14.3$ meV, (c) $\Delta = 34$ meV, and (d) $\Delta = 54$ meV.

shows the electric field envelope obtained from Eq. (2). Using this field, we compute the time evolution of the ground- and excited-state amplitudes of the helium atom. The corresponding state populations, $P_g = |c_g|^2$, $P_e = |c_e|^2$ and ionization $= 1 - P_g - P_e$, are presented in Fig. 2(b). To quantify how significantly the femtosecond laser pulses change the energy level structure, we show the relative dynamical Stark shift, i.e., the difference between the ac Stark shift of the ground state and the $1s2s\ ^1S_0$ excited state as a function of pump pulse intensity for a fixed pulse bandwidth of 9 meV in Fig. 2(c). This shows that due to the strong light-atom interaction, the relative Stark shift is onf the order of meV and is comparable to the bandwidth of the pump pulse. Intuitively, the time-dependent relative ac Stark shift spans the bandwidth of the pump pulse during the excitation. When the magnitude of this relative Stark shift becomes comparable to the pulse bandwidth, the conditions for maximum population transfer are met. This behavior is evident in Fig. 2(d), which shows the excited-state population as a function of laser intensity and pulse bandwidth. For a pulse intensity of $\sim$10 TW/cm^2 and a spectral bandwidth of 9 meV (corresponding to a pulse duration of approximately 200 fs FWHM), the population transfer reaches about 28%. At this intensity, the relative ac Stark shift closely matches the pulse bandwidth, as illustrated in Fig. 2(c). These parameters are experimentally accessible with tabletop femtosecond laser systems using, for example, the RDW technique [42–48]. The dashed line in Fig. 2(d) marks the contour corresponding to an experimentally feasible pulse energy of 10 μJ focused to a 50 μm spot diameter. However, at such high intensities, photoionization starts becoming a limiting factor, reducing the excited-state population particularly for long pulses, where the long-time light-atom interaction further enhances ionization losses, as shown in Fig. 2(e). We also evaluate the two-photon excitation rate, defined as the excitation probability divided by the FWHM pulse width. As shown in Fig. 2(f), for the intensity and bandwidth parameters specified above, the excitation rate is $\sim 2 \times 10^{12} \mathrm{s}^{-1}$ atom^{-1}. Unlike in SCRAP [33–35], where laser-induced continuum structure is used to suppress ionization, we find that broadband femtosecond pulses can still produce high excitation probabilities even in the presence of strong ionization rates.

Broadband laser pulses have been previously employed for efficient multiphoton excitation processes [53–55]. Their large spectral bandwidth provides multiple excitation pathways, thereby enhancing the overall multiphoton transition probability. The two-photon excitation probability can be calculated using second-order perturbation theory and is proportional to the self-convolution of the spectrum of the broadband fields:

$$P_{eg} \propto \left| \int d\omega E(\omega_{eg} - \omega) E(\omega_{eg} + \omega) \right|^2. \tag{12}$$

Equation (12) indicates that the two-photon excitation probability arises from the coherent sum of all possible frequency pathways within the pulse bandwidth. As a result, the excitation probability remains remarkably high for appropriately chosen values of detuning, intensity, and bandwidth, as illustrated in Fig. 3.

IV. XUV-IR TWO-COLOR SCHEME

XUV femtosecond laser pulses have been generated using free electron lasers (FELs) for several decades [56,57].

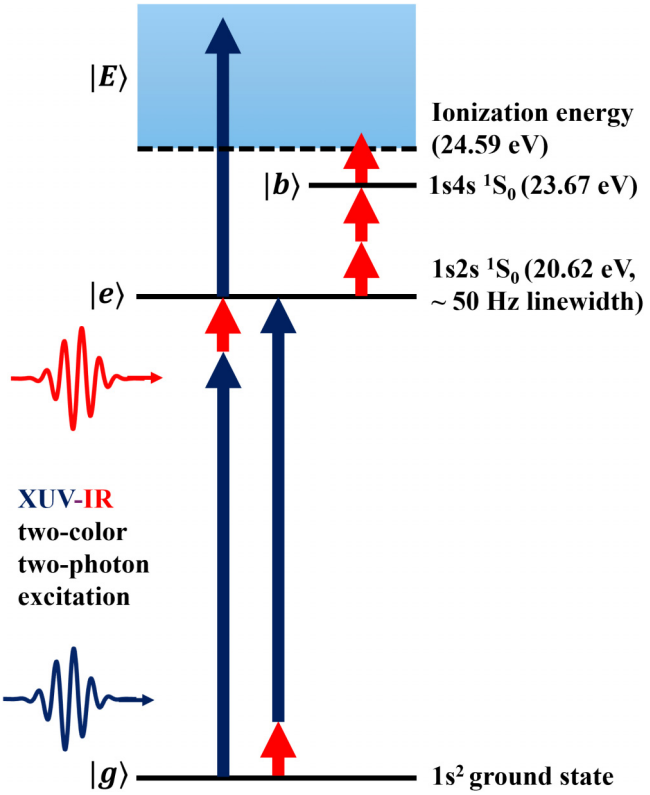


FIG. 4. Two-color two-photon excitation scheme in a helium atom. There are two possible combinations of XUV and IR photons shown, which lead to two-photon excitation. IR photon energy is selected such that it is lower than the energy needed to one-photon photoionize the $1s2s$ state. However, three-photon ionization is possible with a two-photon resonance between $1s2s$ and $1s4s$ states as shown.

Recent advances in FEL technology have substantially increased the photon flux of these pulses [58,59], making them highly suitable for multiphoton excitation experiments.

In the previous section, we examined the one-color (120 nm) two-photon excitation scheme, which, despite significant photoionization, demonstrated efficient population transfer in helium. Here, we propose a two-color approach to further reduce the photoionization rate. In this scheme, a broadband XUV pulse is employed in combination with a near-IR pulse for two-color two-photon excitation, as illustrated in Fig. 4. The IR pulse is chosen so that it lacks sufficient energy to directly ionize the $1s2s$ state. However, multiphoton ionization of the excited state can still occur via the $1s4s$ intermediate state, as also indicated in Fig. 4. Since the photoionization cross section generally decreases with increasing photon energy [60,61], the photoionization rate of the $1s2s$ state due to the XUV pulse, calculated using Eq. (11), is an order of magnitude smaller than that for the 120 nm pulse.

For this scheme, we can modify the wave function (3) as

$$|\psi\rangle = c_g e^{-i\omega_g t}|g\rangle + c_e e^{-i\omega_c t}|e\rangle + c_b e^{-i\omega_b t}|b\rangle + \sum_m c_m e^{-i\omega_m t}|m\rangle + \int dE\; c_E(t) e^{-i\omega_E t}|E\rangle. \quad (13)$$

Here, $|b\rangle$ denotes the state $1s4s\ {}^1S_0$, which is two-photon resonant with the state $1s2s\ {}^1S_0$ for the IR pulse. Following the derivation in Sec. II, the evolution of the coefficients can be written within the RWA and two-photon RWA as

$$i\begin{pmatrix}\dot{c}_g\\ \dot{c}_e\\ \dot{c}_b\end{pmatrix} = \begin{pmatrix} S_g^1(t)+S_g^2(t) & \left(\frac{\Omega_{ge}^{21}}{2}+\frac{\Omega_{ge}^{12}}{2}\right)^* e^{i\Delta_{eg}t} & 0 \\ \left(\frac{\Omega_{ge}^{21}}{2}+\frac{\Omega_{ge}^{12}}{2}\right)e^{-i\Delta_{eg}t} & S_e^1(t)+S_e^2(t)+\frac{\delta E_e^1}{\hbar}-\frac{i}{2}\Gamma_e^1 & \frac{\Omega_{be}^*}{2}e^{i\Delta_{be}t} \\ 0 & \frac{\Omega_{be}}{2}e^{-i\Delta_{be}t} & S_b^1(t)+S_b^2(t)+\frac{\delta E_b^2}{\hbar}-\frac{i}{2}\Gamma_b^2 \end{pmatrix}\begin{pmatrix}c_g\\ c_e\\ c_b\end{pmatrix}, \quad (14)$$

where $S_{g/e/b}^{1(2)}$ denote the Stark shifts of the ground, $1s2s\ {}^1S_0$, and $1s4s\ {}^1S_0$ states induced by pulses ω_1 and ω_2, corresponding to the XUV and IR photon energies, respectively. The two-photon Rabi frequencies Ω_{ge}^{12} and Ω_{ge}^{21} correspond to the two possible excitation pathways depicted in Fig. 4, while Ω_{be} represents the two-photon Rabi frequency for the $1s2s \rightarrow 1s4s$ transition. The two-photon detunings are defined as $\Delta_{eg} = (\omega_1 + \omega_2) - \omega_{eg}$ and $\Delta_{be} = 2\omega_2 - \omega_{be}$. Since IR ($\omega_2$) does not have sufficient energy to photoionize the $1s2s$ state, the energy shift δE_e^1 and the photoionization rate Γ_e^1 are associated with the XUV (ω_1) pulse only. In contrast, the IR pulse can photoionize the $1s4s$ state, so δE_b^2 and Γ_b^2 correspond to the IR-induced effects. Single-photon ionization of the $1s4s$ state by the XUV pulse is neglected because it is orders of magnitude smaller than that induced by the IR pulse. For detailed expressions of these quantities, see Appendix B.

For the numerical calculations, we chose $\hbar\omega_1 = 19.06\,\text{eV}$ (~65 nm, XUV) and $\hbar\omega_2 = 1.54\,\text{eV}$ (~800 nm, IR). Figure 5 shows the excited-state population as a function of IR pulse intensity and pulse width for various values of XUV intensities and pulse widths. This two-color scheme demonstrates that, with appropriately chosen pulse parameters, population transfer efficiencies of up to 70% can be achieved. The populations shown in Fig. 5 correspond to pulse parameters that are currently experimentally accessible at the FLASH FEL [59].

V. SUMMARY

In conclusion, we have presented a detailed theoretical study of two-photon excitation in helium using broadband femtosecond laser pulses to enhance population transfer efficiency to an ultranarrow linewidth state. We showed that the presence of multiple excitation pathways and the broad spectral bandwidth can compensate for both the dynamical Stark shift and the large photoionization rates, thereby significantly increasing the transfer efficiency from the ground state to the

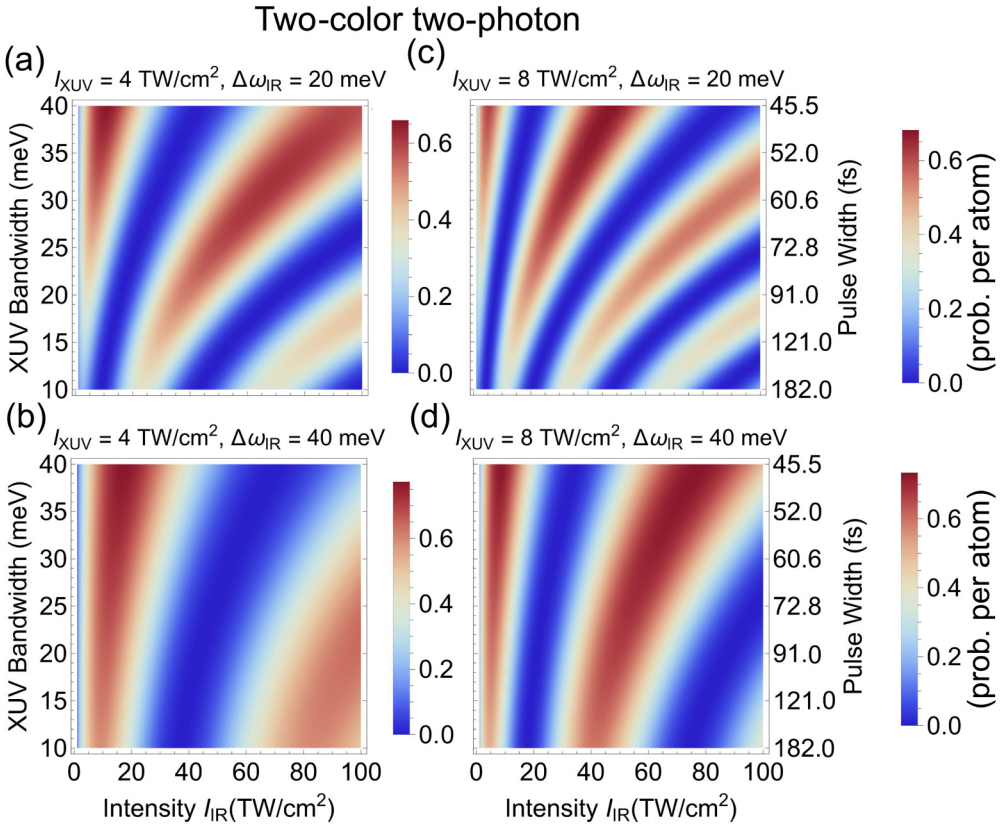


FIG. 5. The excitation probability as a function of IR pulse (ω_2) intensity and width for XUV pulse. (a) XUV intensity = 4 TW/cm^2 and IR bandwidth = 20 meV (pulse width ~91 fs), (b) XUV intensity = 4 TW/cm^2 and IR bandwidth = 40 meV (pulse width ~45 fs), (c) XUV intensity = 8 TW/cm^2 and IR bandwidth = 20 meV (pulse width ~91 fs), and (d) XUV intensity = 8 TW/cm^2 and IR bandwidth = 40 meV (pulse width ~45 fs).

$1s2s$ state. For the 120 nm two-photon excitation scheme, we mapped the excited-state population in the intensity-bandwidth parameter space and found that populations >25% are achievable with experimentally accessible laser parameters. Finally, we proposed a two-color two-photon excitation scheme employing an XUV and an IR pulse. Our calculations show that, under experimentally realizable parameters, this scheme can achieve excited-state populations of ~70%. This approach opens avenues for efficiently populating ultranarrow linewidth atomic states with broadband lasers, paving the path for simplified and more versatile control schemes beyond traditional adiabatic passage techniques such as STIRAP [30–32] and SCRAP [33–35]. In the case of helium atoms, as demonstrated in this study, and in heliumlike systems, such a high excitation probability of the 1s2s $^1S_0$ state could lead to the generation of attosecond bandwidth entangled photons with high rates [26].

ACKNOWLEDGMENTS

We gratefully acknowledge support from the W. M. Keck Foundation. We thank Professor Francis Robicheaux, Purdue University, for insightful discussions.

DATA AVAILABILITY

The data that support the findings of this article are not publicly available upon publication because it is not technically feasible and/or the cost of preparing, depositing, and hosting the data would be prohibitive within the terms of this research project. The data are available from the authors upon reasonable request.

APPENDIX A: DERIVATION OF EFFECTIVE HAMILTONIAN FOR TWO-PHOTON 120 NM EXCITATION SCHEME

The time-dependent Schrodinger equation with laser-atom interaction can be written as

$$\frac{\partial|\psi\rangle}{\partial t} = (H_0 - \boldsymbol{\mu}\cdot\boldsymbol{E_p}(t))|\psi\rangle, \tag{A1}$$

where H_0 is the field-free Hamiltonian of the helium atom and $-\boldsymbol{\mu}\cdot\boldsymbol{E_p}(t)$ is the time-dependent Hamiltonian within the dipole approximation. Putting in Eq. (3), the above time-dependent Schrodinger equation becomes Eq. (4). The energy difference between states m and j is $\omega_{mj} = \omega_m - \omega_j$ and V_{mj} are the elements of the interaction matrix and are defined as

$$V_{mj} = \langle m|V(t)|j\rangle = -\sum_j \frac{\mu^P_{mj}}{2}\left(\varepsilon_P e^{-i\omega_P t} + \varepsilon^*_P e^{i\omega_P t}\right), \tag{A2}$$

where $\mu^P_{mj} = \langle m|\boldsymbol{\mu}\cdot\boldsymbol{e}_P|j\rangle$ are the transition dipole matrix elements. The off-resonant states $c_m(t)$ are calculated by

TABLE I. List of all the quantities that are used in Eq. (7), where E_0 is the electric field corresponding to the intensity I_0. The last two columns are the values for $I_0 = 10\,\mathrm{TW/cm^2}$ in atomic units and SI units, respectively.

Symbols	References	Expression (in a.u.)	Values for $I_0 = 10\,\mathrm{TW/cm^2}$ (in a.u.)	Values for $I_0 = 10\,\mathrm{TW/cm^2}$ (in THz)
S_g	Equation (8)	$-0.424\,664E_0^2$	−0.000 1209 79	−5.0015
S_e	Equation (8)	$1.13668E_0^2$	0.000 323 822	13.3872
Ω_{ge}^P	Equation (9)	$0.886\,278E_0^2$	0.000 252 485	10.4381
$\delta E_e/\hbar$	Equation (10)	$0.840\,524E_0^2$	0.000 239 451	9.8992
Γ_e	Equation (11)	$0.869\,215E_0^2$	0.000 247 624	10.2371

integrating Eq. ((7c)) on both sides,

$$c_j(t) = -\sum_j \frac{c_j \mu_{mj}^P}{2} \int dt \left(\varepsilon_P e^{-i(\omega_P-\omega_{mj})t} + \varepsilon_P^* e^{i(\omega_P+\omega_{mj})t}\right). \tag{A3}$$

Using adiabatic elimination, this coefficient can be approximated in the analytical form shown in Eq. (5). The adiabatic elimination approximation has previously been shown to be valid for broadband femtosecond pulses [50]. Substituting Eq. (5) into Eq. ((4a)),

$$i\hbar \dot{c}_g(t) = \sum_m \sum_j \frac{c_j \mu_{mj}^P}{2\hbar} \left[\frac{\varepsilon_P e^{-i(\omega_P-\omega_{mj})t}}{\omega_{mj}-\omega_P} + \frac{\varepsilon_P^* e^{i(\omega_P+\omega_{mj})t}}{\omega_{mj}+\omega_P}\right] \times e^{-i\omega_{mg}t}\left[-\frac{\mu_{gm}^P}{2}\left(\varepsilon_P e^{-i\omega_P t} + \varepsilon_P^* e^{i\omega_P t}\right)\right]. \tag{A4}$$

Using RWA and two-photon RWA, the terms that oscillate faster than the two-photon detuning $\Delta = 2\omega_P - \omega_{eg}$ to give

$$i\hbar \dot{c}_g(t) = -\sum_m c_g(t) \frac{\mu_{mg}^P \mu_{gm}^P}{4\hbar}\left[\frac{|\varepsilon_P|^2}{(\omega_{mg}-\omega_P)} + \frac{|\varepsilon_P|^2}{(\omega_{mg}+\omega_P)}\right] - \sum_m c_e(t) \frac{\mu_{mg}^P \mu_{gm}^P}{4\hbar} \frac{\varepsilon_P^{*2}(t)}{\omega_{me}+\omega_p} e^{-i(\omega_{eg}-2\omega_P)t}, \tag{A5}$$

$$i\dot{c}_g \approx -\sum_m \frac{\left|\mu_{mg}^P\right|^2}{2\hbar^2}|\varepsilon_P|^2 \frac{\omega_{mg}}{\omega_{mg}^2-\omega_P^2} c_g(t) - \sum_m \frac{\mu_{gm}^P \mu_{me}^P}{4\hbar^2} \frac{\varepsilon_P^{*2}(t)}{\omega_{mg}-\omega_P} e^{i\Delta t} c_e(t). \tag{A6}$$

In the last step, $\omega_{me} + \omega_P = \omega_m - \omega_e + \omega_P \approx \omega_m - (\omega_g + 2\omega_P) + \omega_P = \omega_{mg} - \omega_P$ relations have been used. Similarly, for the coefficient for the excited state,

$$i\dot{c}_e \approx -\sum_m \frac{\left|\mu_{me}^P\right|^2}{2\hbar^2}|\varepsilon_P|^2 \frac{\omega_{me}}{\omega_{me}^2-\omega_P^2} c_e(t) - \sum_m \frac{\mu_{em}^P \mu_{mg}^P}{4\hbar^2} \frac{\varepsilon_P^2(t)}{\omega_{me}-\omega_P} e^{-i\Delta t} c_g(t) + \int dE\, c_E(t) e^{-i\omega_{eE}t} V_{eE}(t). \tag{A7}$$

The amplitudes corresponding to the continuum states can be calculated using Eq. (6). Substituting this into the last term of Eq. (A7), which corresponds to the coupling between excited state $1s2s$ and continuum state, gives

$$\int dE\, c_E(t) e^{-i\omega_{Ee}t} V_{eE}(t) = \frac{1}{2i\hbar} \int dE \int_{-\infty}^{t} dt' c_e(t') \mu_{Ee}^P \times \left[\varepsilon_P e^{-i(\omega_P-\omega_{Ee})t'} + \varepsilon_P^* e^{i(\omega_P+\omega_{Ee})t'}\right] \times \frac{\mu_{eE}^P}{2}\left[\varepsilon_P e^{-i(\omega_P+\omega_{Ee})t} + \varepsilon_P^*(t) e^{i(\omega_P-\omega_{Ee})t}\right]. \tag{A8}$$

Within RWA, the terms containing detuning $\mathcal{D}_{\alpha j} = \omega_E - \omega_\alpha - \omega_j$ will be considered,

$$\int dE\, c_E(t) e^{-i\omega_{Ee}t} V_{eE}(t) = \frac{1}{4i\hbar} \int dE \int_{-\infty}^{t} dt' c_e(t') |\mu_{eE}^P|^2 |\varepsilon_P|^2 e^{-i\mathcal{D}_{Pe}(t-t')} \approx \frac{1}{4i\hbar} \int dE \left[c_e(t)|\mu_{eE}^P|^2|\varepsilon_P|^2 \int_0^\infty dT e^{-i\mathcal{D}_{Pe}T}\right], \tag{A9}$$

where in the last step we have used the Markovian approximation such that $c_j(t') \approx c_j(t)$ [51] and $T = t - t'$. Using the relation,

$$\int_0^\infty dT e^{-i\mathcal{D}_{\alpha j}T} = -i\mathcal{P}\left(\frac{1}{\mathcal{D}_{\alpha j}}\right) + \pi\delta(\mathcal{D}_{\alpha j}), \tag{A10}$$

$$\int dE\, c_E(t) e^{-i\omega_{Ee}t} V_{eE}(t) = -c_e(t)\left[\mathcal{P}\int dE \frac{\left|\mu_{eE}^P\right|^2|\varepsilon_P|^2}{4\hbar\mathcal{D}_{Pe}} + \frac{\pi\hbar|\varepsilon_P|^2}{4i\hbar}\left|\mu_{eE=\hbar\omega_P+\hbar\omega_e}^P\right|^2\right]. \tag{A11}$$

The dynamical energy shifts δE_e and the photoionization rate Γ_e^P of the excited state $1s2s$ are defined in Eqs. (10) and (11), respectively. Substituting these relations into Eq. (A7) renders Eqs. (A6) and (A7) as a coupled set of differential equations for c_g and c_e. These equations can be expressed in the compact matrix form given in Eq. (7). The numerical solution of this equation, along with the computational details and results, is presented in Sec. III. The values of the quantities derived above for peak pump intensity of 10 TW/cm^2 have been listed in Table I.

APPENDIX B: DERIVATION OF EFFECTIVE HAMILTONIAN FOR XUV-IR TWO-COLOR SCHEME

Two-photon excitation can also be realized using a two-color scheme, as described in Sec. IV. However, this

TABLE II. List of all the quantities that are used in Eq. (14), where $E_{\rm XUV}$ and $E_{\rm IR}$ are the electric fields corresponding to the intensities of XUV pulse $I_{\rm XUV}$ and IR pulse $I_{\rm IR}$, respectively. The superscripts 1 and 2 in the symbol corresponds to the XUV, IR, respectively. The last two columns are their values for $I_{\rm XUV} = 4$ TW/cm^2 and $I_{\rm IR} = 10$ TW/cm^2 in atomic units and SI units.

Symbols	References	Expression (in a.u.)	Values (in a.u.)	Values (in THz)
S_g^1	Equation (B3)	$-1.060\,74E_{\rm XUV}^2$	$-0.000\,1208\,75$	-4.9971
S_g^2	Equation (B3)	$-0.355\,442E_{\rm IR}^2$	$-0.000\,101\,259$	-4.1862
S_e^1	Equation (B3)	$0.324\,151E_{\rm XUV}^2$	0.000 036 9381	1.527 07
S_e^2	Equation (B3)	$24.7805E_{\rm IR}^2$	0.007 059 53	291.851
S_b^1	Equation (B3)	$0.409\,08E_{\rm XUV}^2$	0.000 046 616	1.927 17
S_b^2	Equation (B3)	$65.2027E_{\rm IR}^2$	0.018 5751	767.921
Ω_{ge}^{12}	Equation (B4)	$0.437\,418E_{\rm XUV}E_{\rm IR}$	0.000 078 8122	3.2582
Ω_{ge}^{21}	Equation (B4)	$6.1548E_{\rm XUV}E_{\rm IR}$	0.001 108 95	45.8453
Ω_{be}	Equation (B9)	$-8.573\,07E_{\rm IR}^2$	$-0.002\,442\,32$	-100.969
$\delta E_e^1/\hbar$	Equation (B5)	$0.366\,396E_{\rm XUV}^2$	0.000 041 752	1.726 08
$\delta E_b^2/\hbar$	Equation (B7)	$11.6423E_{\rm IR}^2$	0.003 316 68	137.116
Γ_e	Equation (B6)	$0.127\,529\,E_{\rm XUV}^2$	0.000 014 5323	0.600 79
Γ_b	Equation (B8)	$29.711\,E_{\rm IR}^2$	0.008 464 15	349.92

introduces additional pathways that couple the $1s2s$ state to the continuum through multiphoton excitation. The corresponding wave function is shown in Eq. (13). Substituting this into Eq. (A1), where $V(t) = -\boldsymbol{\mu}\cdot(\boldsymbol{E}_1(t)+\boldsymbol{E}_2(t))$, we get a set of equations of complex amplitude similar to Eq. (4),

$$i\hbar\dot{c}_g(t) = \sum_m c_m(t)e^{-i\omega_{mg}t}V_{gm}(t), \tag{B1a}$$

$$i\hbar\dot{c}_e(t) = \sum_m c_m(t)e^{-i\omega_{me}t}V_{em}(t) + \int dE\, c_E(t)e^{-i\omega_{eE}t}V_{eE}(t), \tag{B1b}$$

$$i\hbar\dot{c}_b(t) = \sum_m c_m(t)e^{-i\omega_{mb}t}V_{bm}(t) + \int dE\, c_E(t)e^{-i\omega_{bE}t}V_{bE}(t), \tag{B1c}$$

$$i\hbar\dot{c}_m(t) = \sum_{j=g,e,b} c_j(t)e^{i\omega_{mj}t}V_{mj}(t), \tag{B1d}$$

$$i\hbar\dot{c}_E(t) = c_e(t)e^{i\omega_{Ee}t}V_{Ee}(t) + c_b(t)e^{i\omega_{Eb}t}V_{Eb}(t), \tag{B1e}$$

where $\boldsymbol{E}_{1(2)}$ denotes the electric field of the XUV(IR) pulse. Rapidly oscillating nonresonant amplitudes can be obtained using adiabatic elimination, as discussed in Appendix A. A similar derivation is performed to obtain the amplitudes of state $|g\rangle$,

$$\begin{aligned} i\dot{c}_g \approx &-\sum_m\sum_{\alpha=1,2}\frac{\left|\mu_{mg}^{\alpha}\right|^2}{2\hbar^2}|\varepsilon_\alpha|^2\frac{\omega_{mg}}{\omega_{mg}^2-\omega_\alpha^2}c_g(t) \\ &-\sum_m\left[\frac{\mu_{gm}^1\mu_{me}^2}{4\hbar^2}\frac{\varepsilon_1^*(t)\varepsilon_2^*(t)}{\omega_{mg}-\omega_1}+\frac{\mu_{gm}^2\mu_{me}^1}{4\hbar^2}\frac{\varepsilon_2^*\varepsilon_1^*}{\omega_{mg}-\omega_2}\right] \\ &\times e^{i\Delta_{eg}t}c_e(t), \end{aligned} \tag{B2}$$

where $\Delta_{eg} = (\omega_1+\omega_2)-\omega_{eg}$ is the two-photon detuning. A similar relation can also be derived for the time evolution of the amplitudes c_e and c_b. The dynamical Stark shift of the jth $= \{g, e, b\}$ states corresponding to the XUV (IR) pulse is given by

$$S_j^{1(2)}(t) = -\sum_m \frac{\left|\mu_{mj}^{1(2)}\right|^2}{2\hbar^2}|\varepsilon_{1(2)}|^2\frac{\omega_{mj}}{\omega_{mj}^2-\omega_{1(2)}^2}. \tag{B3}$$

The two-color two-photon Rabi frequencies for two possible pathways are defined as

$$\Omega_{ge}^{12(21)} = -\sum_m \frac{\mu_{em}^{1(2)}\mu_{mg}^{2(1)}}{2\hbar^2}\frac{\varepsilon_{1(2)}\varepsilon_{2(1)}}{\omega_{mg}-\omega_{1(2)}}. \tag{B4}$$

The equation for $\dot{c}_e$ also includes contributions from the dynamical energy shifts and photoionization of the $1s2s$ state ($|e\rangle$), arising from its coupling to the continuum via the XUV pulse only:

$$\delta E_e^1 = -\mathcal{P}\int dE\,\frac{1}{4\hbar}\frac{\left|\mu_{eE}^1\right|^2|\varepsilon_1|^2}{\omega_E-\omega_1-\omega_e}, \tag{B5}$$

$$\Gamma_e^1(t) = \frac{\pi}{2\hbar}|\varepsilon_1|^2|\langle e|\mu\cdot\hat{\epsilon}_1|E=\hbar\omega_1+\hbar\omega_e\rangle|^2. \tag{B6}$$

However, the evolution of the amplitude c_b, corresponding to the $1s4s$ state, includes both the dynamical energy shift and photoionization induced by the IR pulse only:

$$\delta E_b^2 = -\mathcal{P}\int dE\,\frac{1}{4\hbar}\frac{\left|\mu_{bE}^2\right|^2|\varepsilon_2|^2}{\omega_E-\omega_2-\omega_b}, \tag{B7}$$

$$\Gamma_b^2(t) = \frac{\pi}{2\hbar}|\varepsilon_2|^2|\langle b|\mu\cdot\hat{\epsilon}_2|E=\hbar\omega_2+\hbar\omega_b\rangle|^2. \tag{B8}$$

Finally, the states $|e\rangle$ and $|b\rangle$ are coupled via the IR two-photon Rabi frequency,

$$\Omega_{eb} = -\sum_m \frac{\mu_{bm}^2\mu_{me}^2}{2\hbar^2}\frac{\varepsilon_2^2(t)}{\omega_{me}-\omega_2}. \tag{B9}$$

Combining all contributions, we arrive at Eq. (14). Table II lists all the quantities derived here for the peak XUV intensity of 4 TW/cm^2 and peak IR intensity of 10 TW/cm^2.

[1] X. Shi, J. Sinanan-Singh, K. DeBry, S. L. Todaro, I. L. Chuang, and J. Chiaverini, Long-lived metastable-qubit memory, Phys. Rev. A **111**, L020601 (2025).

[2] S. Pucher, V. Klüsener, F. Spriestersbach, J. Geiger, A. Schindewolf, I. Bloch, and S. Blatt, Fine-structure qubit encoded in metastable strontium trapped in an optical lattice, Phys. Rev. Lett. **132**, 150605 (2024).

[3] T. P. Harty, D. T. C. Allcock, C. J. Ballance, L. Guidoni, H. A. Janacek, N. M. Linke, D. N. Stacey, and D. M. Lucas, High-fidelity preparation, gates, memory, and readout of a trapped-ion quantum bit, Phys. Rev. Lett. **113**, 220501 (2014).

[4] G. Unnikrishnan, P. Ilzhöfer, A. Scholz, C. Hölzl, A. Götzelmann, R. K. Gupta, J. Zhao, J. Krauter, S. Weber, N. Makki, H. P. Büchler, T. Pfau, and F. Meinert, Coherent control of the fine-structure qubit in a single Alkaline-earth atom, Phys. Rev. Lett. **132**, 150606 (2024).

[5] Y. Wang, M. Um, J. Zhang, S. An, M. Lyu, J.-N. Zhang, L.-M. Duan, D. Yum, and K. Kim, Single-qubit quantum memory exceeding ten-minute coherence time, Nat. Photonics **11**, 646 (2017).

[6] P. Wang, C.-Y. Luan, M. Qiao, M. Um, J. Zhang, Y. Wang, X. Yuan, M. Gu, J. Zhang, and K. Kim, Single ion qubit with estimated coherence time exceeding one hour, Nat. Commun. **12**, 233 (2021).

[7] A. Aeppli, K. Kim, W. Warfield, M. S. Safronova, and J. Ye, Clock with 8×10^{-19} systematic uncertainty, Phys. Rev. Lett. **133**, 023401 (2024).

[8] M. A. Bohman, S. G. Porsev, D. B. Hume, D. R. Leibrandt, and M. S. Safronova, Enhancing divalent optical atomic clocks with the $^1S_0 \leftrightarrow {}^3P_2$ transition, Phys. Rev. A **108**, 053120 (2023).

[9] S. R. Jefferts, T. P. Heavner, T. E. Parker, J. H. Shirley, E. A. Donley, N. Ashby, F. Levi, D. Calonico, and G. A. Costanzo, High-accuracy measurement of the blackbody radiation frequency shift of the ground-state hyperfine transition in ^{133}Cs, Phys. Rev. Lett. **112**, 050801 (2014).

[10] K. Beeks, T. Sikorsky, T. Schumm, J. Thielking, M. V. Okhapkin, and E. Peik, The thorium-229 low-energy isomer and the nuclear clock, Nat. Rev. Phys. **3**, 238 (2021).

[11] C. Zhang, T. Ooi, J. S. Higgins, J. F. Doyle, L. von der Wense, K. Beeks, A. Leitner, G. A. Kazakov, P. Li, P. G. Thirolf, T. Schumm, and J. Ye, Frequency ratio of the ^{229m}Th nuclear isomeric transition and the ^{87}Sr atomic clock, Nature (London) **633**, 63 (2024).

[12] J. Shapiro and G. Breit, Metastability of 2*s* states of hydrogenic atoms, Phys. Rev. **113**, 179 (1959).

[13] M. H. Prior, Lifetime of the 2*s* state of He^+, Phys. Rev. Lett. **29**, 611 (1972).

[14] C. A. Kocher, J. E. Clendenin, and R. Novick, Lifetime of the $2^2S_{\frac{1}{2}}$ state of singly ionized helium, Phys. Rev. Lett. **29**, 615 (1972).

[15] E. A. Hinds, J. E. Clendenin, and R. Novick, Decay rate of the $2^2S_{\frac{1}{2}}$ state of singly ionized helium, Phys. Rev. A **17**, 670 (1978).

[16] R. S. Van Dyck, C. E. Johnson, and H. A. Shugart, Radiative lifetime of the 2^1S_0 metastable state of helium, Phys. Rev. A **4**, 1327 (1971).

[17] S. S. Hodgman, R. G. Dall, L. J. Byron, K. G. H. Baldwin, S. J. Buckman, and A. G. Truscott, Metastable helium: A new determination of the longest atomic excited-state lifetime, Phys. Rev. Lett. **103**, 053002 (2009).

[18] E. A. Hildum, U. Boesl, D. H. McIntyre, R. G. Beausoleil, and T. W. Hansch, Measurement of the 1*S*-2*S* frequency in atomic hydrogen, Phys. Rev. Lett. **56**, 576 (1986).

[19] M. Niering, R. Holzwarth, J. Reichert, P. Pokasov, T. Udem, M. Weitz, T. W. Hänsch, P. Lemonde, G. Santarelli, M. Abgrall, P. Laurent, C. Salomon, and A. Clairon, Measurement of the hydrogen 1*S*-2*S* transition frequency by phase coherent comparison with a microwave cesium fountain clock, Phys. Rev. Lett. **84**, 5496 (2000).

[20] C. G. Parthey, A. Matveev, J. Alnis, B. Bernhardt, A. Beyer, R. Holzwarth, A. Maistrou, R. Pohl, K. Predehl, T. Udem, T. Wilken, N. Kolachevsky, M. Abgrall, D. Rovera, C. Salomon, P. Laurent, and T. W. Hänsch, Improved measurement of the hydrogen 1*S*–2*S* transition frequency, Phys. Rev. Lett. **107**, 203001 (2011).

[21] M. Ahmadi, B. X. R. Alves, C. J. Baker, W. Bertsche, A. Capra, C. Carruth, C. L. Cesar, M. Charlton, S. Cohen, R. Collister, *et al.*, Characterization of the 1*S*–2*S* transition in antihydrogen, Nature (London) **557**, 71 (2018).

[22] M. Lipeles, R. Novick, and N. Tolk, Direct detection of two-photon emission from the metastable state of singly ionized helium, Phys. Rev. Lett. **15**, 690 (1965).

[23] A. Dalgarno and D. R. Bates, Two-photon decay of singlet metastable helium, Mon. Not. R. Astron. Soc. **131**, 311 (1966).

[24] G. W. F. Drake, G. A. Victor, and A. Dalgarno, Two-photon decay of the singlet and triplet metastable states of helium-like ions, Phys. Rev. **180**, 25 (1969).

[25] A. T. Bondy, D. C. Morton, and G. W. F. Drake, Two-photon decay rates in heliumlike ions: Finite-nuclear-mass effects, Phys. Rev. A **102**, 052807 (2020).

[26] Y. Wang, S. Pandey, C. H. Greene, and N. Shivaram, Attosecond entangled photons from two-photon decay of metastable atoms: A source for attosecond experiments and beyond, Phys. Rev. Res. **4**, L032038 (2022).

[27] A. Grinin, A. Matveev, D. C. Yost, L. Maisenbacher, V. Wirthl, R. Pohl, T. W. Hänsch, and T. Udem, Two-photon frequency comb spectroscopy of atomic hydrogen, Science **370**, 1061 (2020).

[28] T. Mossberg, A. Flusberg, R. Kachru, and S. R. Hartmann, Trilevel echoes, Phys. Rev. Lett. **39**, 1523 (1977).

[29] J.-H. Choi, B. Knuffman, T. C. Liebisch, A. Reinhard, and G. Raithel, Cold Rydberg atoms, in *Advances in Atomic, Molecular, and Optical Physics*, Vol. 54 (Academic Press, 2007), pp. 131–202.

[30] U. Gaubatz, P. Rudecki, S. Schiemann, and K. Bergmann, Population transfer between molecular vibrational levels by stimulated Rraman scattering with partially overlapping laser fields. A new concept and experimental results, J. Chem. Phys. **92**, 5363 (1990).

[31] K. Bergmann, H. Theuer, and B. W. Shore, Coherent population transfer among quantum states of atoms and molecules, Rev. Mod. Phys. **70**, 1003 (1998).

[32] N. V. Vitanov, A. A. Rangelov, B. W. Shore, and K. Bergmann, Stimulated Rraman adiabatic passage in physics, chemistry, and beyond, Rev. Mod. Phys. **89**, 015006 (2017).

[33] L. P. Yatsenko, B. W. Shore, T. Halfmann, K. Bergmann, and A. Vardi, Source of metastable H(2*s*) atoms using the Stark chirped rapid-adiabatic-passage technique, Phys. Rev. A **60**, R4237(R) (1999).

[34] L. P. Yatsenko, V. R. Romanenko, B. W. Shore, T. Halfmann, and K. Bergmann, Two-photon excitation of the metastable 2*s* state of hydrogen assisted by laser-induced chirped Stark shifts and continuum structure, Phys. Rev. A **71**, 033418 (2005).

[35] T. Rickes, L. P. Yatsenko, S. Steuerwald, T. Halfmann, B. W. Shore, N. V. Vitanov, and K. Bergmann, Efficient adiabatic population transfer by two-photon excitation assisted by a laser-induced Stark shift, J. Chem. Phys. **113**, 534 (2000).

[36] E. Appi, C. C. Papadopoulou, J. L. Mapa, N. Wesavkar, C. Jusko, P. Mosel, S. Ališauskas, T. Lang, C. M. Heyl, B. Manschwetus, *et al.*, A synchronized VUV light source based on high-order harmonic generation at FLASH, Sci. Rep. **10**, 6867 (2020).

[37] K. Konishi, D. Akai, Y. Mita, M. Ishida, J. Yumoto, and M. Kuwata-Gonokami, Tunable third harmonic generation in the vacuum ultraviolet region using dielectric nanomembranes, APL Photonics **5**, 066103 (2020).

[38] L. Misoguti, S. Backus, C. G. Durfee, R. Bartels, M. M. Murnane, and H. C. Kapteyn, Generation of broadband VUV light using third-order cascaded processes, Phys. Rev. Lett. **87**, 013601 (2001).

[39] R. Forbes, P. Hockett, Q. Leterrier, and R. Lausten, Efficient (∼10%) generation of vacuum ultraviolet femtosecond pulses via four-wave mixing in hollow-core fibers, Opt. Lett. **49**, 3178 (2024).

[40] J. M. Dudley, G. Genty, and S. Coen, Supercontinuum generation in photonic crystal fiber, Rev. Mod. Phys. **78**, 1135 (2006).

[41] Y.-C. Cheng, C.-H. Lu, Y.-Y. Lin, and A. H. Kung, Supercontinuum generation in a multi-plate medium, Opt. Express **24**, 7224 (2016).

[42] S.-J. Im, A. Husakou, and J. Herrmann, High-power soliton-induced supercontinuum generation and tunable sub-10-fs VUV pulses from Kagome-lattice HC-PCFs, Opt. Express **18**, 5367 (2010).

[43] N. Y. Joly, J. Nold, W. Chang, P. Hölzer, A. Nazarkin, G. K. L. Wong, F. Biancalana, and P. S. J. Russell, Bright spatially coherent wavelength-tunable deep-UV laser source using an Ar-filled photonic crystal fiber, Phys. Rev. Lett. **106**, 203901 (2011).

[44] K. F. Mak, J. C. Travers, P. Hölzer, N. Y. Joly, and P. S. J. Russell, Tunable vacuum-UV to visible ultrafast pulse source based on gas-filled Kagome-PCF, Opt. Express **21**, 10942 (2013).

[45] F. Belli, A. Abdolvand, W. Chang, J. C. Travers, and P. S. Russell, Vacuum-ultraviolet to infrared supercontinuum in hydrogen-filled photonic crystal fiber, Optica **2**, 292 (2015).

[46] F. Köttig, F. Tani, C. M. Biersach, J. C. Travers, and P. S. Russell, Generation of microjoule pulses in the deep ultraviolet at megahertz repetition rates, Optica **4**, 1272 (2017).

[47] A. Ermolov, K. F. Mak, M. H. Frosz, J. C. Travers, and P. S. J. Russell, Supercontinuum generation in the vacuum ultraviolet through dispersive-wave and soliton-plasma interaction in a noble-gas-filled hollow-core photonic crystal fiber, Phys. Rev. A **92**, 033821 (2015).

[48] J. C. Travers, T. F. Grigorova, C. Brahms, and F. Belli, High-energy pulse self-compression and ultraviolet generation through soliton dynamics in hollow capillary fibres, Nat. Photonics **13**, 547 (2019).

[49] M. Aymar, C. H. Greene, and E. Luc-Koenig, Multichannel Rydberg spectroscopy of complex atoms, Rev. Mod. Phys. **68**, 1015 (1996).

[50] B. Kaufman, T. Rozgonyi, P. Marquetand, and T. Weinacht, Adiabatic elimination in strong-field light-matter coupling, Phys. Rev. A **102**, 063117 (2020).

[51] P. L. Knight, M. A. Lauder, and B. J. Dalton, Laser-induced continuum structure, Phys. Rep. **190**, 1 (1990).

[52] A. Tóth, S. Borbély, Y. Zhou, and A. Csehi, Role of dynamic Stark shifts in strong-field excitation and subsequent ionization, Phys. Rev. A **107**, 053101 (2023).

[53] J. N. Bruhnke, E. Olofsson, A. Stenquist, and J. M. Dahlström, Giant counter-rotating oscillations on the attosecond timescale, Phys. Rev. Res. **7**, L042019 (2025).

[54] D. Nobis, H. G. Sansom, and S. W. Magennis, Pulse-shaped broadband multiphoton excitation for single-molecule fluorescence detection in the far field, Methods Appl. Fluoresc. **11**, 017001 (2023).

[55] D. Meshulach and Y. Silberberg, Coherent quantum control of multiphoton transitions by shaped ultrashort optical pulses, Phys. Rev. A **60**, 1287 (1999).

[56] J. Murphy and C. Pellegrini, Free electron lasers for the XUV spectral region, Nucl. Instrum. Methods Phys. Res. Sect. A **237**, 159 (1985).

[57] P. Radcliffe, M. Arbeiter, W. B. Li, S. Düsterer, H. Redlin, P. Hayden, P. Hough, V. Richardson, J. T. Costello, T. Fennel, and M. Meyer, Atomic photoionization in combined intense XUV free-electron and infrared laser fields, New J. Phys. **14**, 043008 (2012).

[58] P. Finetti, H. Höppner, E. Allaria, C. Callegari, F. Capotondi, P. Cinquegrana, M. Coreno, R. Cucini, M. B. Danailov, A. Demidovich, *et al.*, Pulse duration of seeded free-electron lasers, Phys. Rev. X **7**, 021043 (2017).

[59] M. M. Bidhendi, I. J. Bermudez Macias, R. Ivanov, M. V. Yurkov, and S. Düsterer, FEL pulse duration evolution along undulators at FLASH, Appl. Sci. **12**, 7048 (2022).

[60] M. Rafiq, S. Hussain, M. Saleem, M. A. Kalyar, and M. A. Baig, Measurement of photoionization cross section from the 3s3p $^1P_1$ excited state of magnesium, J. Phys. B: At. Mol. Opt. Phys. **40**, 2291 (2007).

[61] G. Reitsma, J. Hummert, J. Dura, V. Loriot, M. J. J. Vrakking, F. Lépine, and O. Kornilov, Delayed relaxation of highly excited cationic states in naphthalene, J. Phys. Chem. A **123**, 3068 (2019).